International Journal of Aeronautical and Space Sciences (2021) 22:751–764
https://doi.org/10.1007/s42405-021-00362-2

IJASS International Journal of Aeronautical and Space Sciences

ORIGINAL PAPER

Design Optimization and Investigation of Aerodynamic Characteristics of Low Reynolds Number Airfoils

Ali Arshad[1] · **Lucas Brandão Rodrigues**[1] · **Iñigo Martínez López**[1]

Received: 13 January 2020 / Revised: 9 December 2020 / Accepted: 25 January 2021 / Published online: 23 February 2021

Abstract
This study aims to develop a simple and efficient design optimization methodology for the low Reynolds number airfoils. XFOIL is used as an aerodynamic solver while modeFRONTIER workflow is employed for the design optimization purpose. The airfoil SG6043 is used as the reference airfoil for optimization due to its common applications when long-endurance characteristics are desired. A simple design optimization methodology with the integration of XFOIL in the modeFRONTIER workflow environment is proposed in this study. The proposed "software integration methodology" demonstrated up to 10% improvement in the optimization parameter which makes it more efficient by reducing the optimization time and steps without unnecessary user intervention which are the limitations conventionally associated with the optimization process. The optimization results are further compared with the results of the numerical simulations. The use of the transition-sensitive turbulence model allowed the evaluation of the behavior of the laminar separation bubble for different angles of attack, observing that it shifts towards the leading edge and has its length reduced as the angle of attack increases. The newly generated airfoil exhibits improved aerodynamic characteristics as compared to the base airfoil. The optimized airfoil can be used in the applications of UAVs as well as in general aviation. Further validation of the airfoil using wind tunnel testing is recommended and planned.

Keywords Airfoil optimization · Low Reynolds number · UAVs · Optimization software integration · Laminar separation bubble

1 Introduction

For over 100 years, airfoil design has captured the interest of researchers and aerodynamicists. Recently attention has turned toward low Reynolds number aerodynamics in an effort to obtain better performance for both military and civilian applications. These applications include UAVs at high altitudes, small UAVs at low altitudes, man-powered aircraft, sailplanes, and wind turbines. The design and evaluation techniques of airfoil sections above chord Reynolds numbers of 500,000 are well developed. Nevertheless, the problems related to boundary layer separations and transition have been found below the Reynolds number of 500,000, such as the formation of laminar separation bubbles, which can significantly reduce the performance of the airfoil [1–3]. Gross and Fasel [2] carried out wind and water tunnel experiments for the NACA 64_3-618 airfoil, during the investigations for the lowest Reynolds number (Re = 64,200), a closed laminar separation bubble was identified near the leading edge for $10^\circ < \alpha < 15^\circ$. The turbulent boundary layer downstream of the bubble was more resistant to separation which yielded a lift recovery for $10^\circ < \alpha < 15^\circ$. As the angle of attack was further increased, the downstream separation and the leading edge bubble merged resulting in an opening up of the leading edge bubble followed by a complete stall of the airfoil.

Potential flow theory is commonly used to evaluate the aerodynamic performance of airfoils, airplanes, wind blades, etc. when speed is preferred over accuracy. Drela [4] presented an analysis and design system for low Reynolds number airfoils called XFOIL. In this system, the potential flow is coupled with viscous models, allowing it to capture viscous effects while maintaining the computational advantages of the potential flow. The boundary layer and transition

✉ Ali Arshad
ali.arshad@rtu.lv

[1] Institute of Aeronautics, Faculty of Mechanical Engineering, Transport, and Aeronautics, Riga Technical University, Riga, Latvia

equations are simultaneously solved with the inviscid flow field, thus, suitable for rapid analysis of low Reynolds number airfoils with separation bubbles. Besides, the grid density must be sufficient to define the surface of the geometry, since XFOIL's formulation is a simple linear-vorticity stream function panel method and the accuracy of results depends on the number of panels. Katz [5] investigated the effect of grid density on computed results using the airfoil NACA4412. The airfoil shape was represented by 10, 24, 50, 100, and 200 elements and the case with 50 panels showed very close results to the experimental data in terms of lift coefficient. Drela [4] also carried out similar experiments using XFOIL with a Joukowsky airfoil represented by 40, 60, 100, and 160 panels. The errors in lift coefficient were 0.766%, 0.34%, 0.175% and 0.085% respectively.

At the same time, multidisciplinary design optimization (MDO) has been used frequently in recent studies. Buckley [6] performed the optimization of a hypothetical aircraft using practical aerodynamic requirements. Tirado [7] carried out an optimization study of an airfoil shape to minimize drag, which is one of the fundamental requirements of any aerodynamic design. Ferreira et al. [8] used optimization techniques to define a family of airfoils for stall regulated VAWT (vertical axis wind turbines). The coupling of numerical optimization tools with computational fluid dynamics has benefited in terms of aerodynamic shape optimization techniques that are efficient at producing configurations with increased performance characteristics at a given operating condition. When one thinks of design optimization, instead of evaluating only one configuration, several configurations need to be evaluated, given the fact that it is an interactive process. In that case, for the design optimization, the time required for the computational simulations to solve the Navier–Stokes equations increases exponentially when compared with a relatively simpler numerical simulation. With that said, at a preliminary stage of design optimization, the coupling of MDO with potential flow methods is considered as the preferred choice due to better time performance, yet providing sufficiently accurate predictions of aerodynamics performance [9]. By doing this, the designer can locate the most promising regions of the design space and then proceed further with computational simulations for more accurate results.

Within the scope of the RANS equations and turbulence models, Langtry–Menter [10] proposed the γ-Reθ transition model using two transport equations for the intermittency while Reθ combined with the shear stress transport turbulence model. The transition model includes two empirical correlations for the onset and length of transition. Such turbulence model is frequently implemented using commercial software such as ANSYS. Hübbe [11] compared the results obtained by Spalart–Allmaras and SST k–ω models and by two transition sensitive models (γ-Reθ and k-kL-ω) for the airfoils E387 and S1223. Only the transition sensitive models captured the formation of laminar separation bubbles, resulting in considerable differences in the lift at high angles of attack. In terms of drag, the transition sensitive models demonstrated lower error than the turbulent flow models when compared with reference data.

Keeping in mind the previous studies as well as the current and future developments of low Reynolds airfoils for specific applications, the authors believe that there is still room for the methodologies that couple MDO and the analysis tools to generate new airfoils based on their practical requirements. The methodologies developed for the new airfoils can be potentially useful in the future low redesigns of the UAVs, wind turbines, human-powered aircraft, and sailplanes. The previous studies, especially of Tirado [7], successfully coupled optimization techniques with far-field analysis to minimize the drag force of NACA0012 airfoil. However, the study was conducted for a relatively higher Reynolds number ($M_\infty = 0.85$) at which the viscous effects are less relevant for the aerodynamic characteristics of the airfoils,hence, an inviscid flow assumption was adopted for the analysis. Additionally, at the higher Reynolds numbers, laminar separation bubbles are unlikely to appear. On the other hand, for the low Re applications, viscous effects are of core importance due to the possible presence of the laminar separation bubble on the surface which significantly influences the aerodynamic characteristics.

Current research in the use of low Reynolds number airfoils is primarily focused on forward flight-style and hovering propellers, wind turbines, and turbomachinery [12–16]. Even though these efforts might improve the propulsive characteristics, the performance of an aircraft is strongly affected by the wing airfoil characteristics. Therefore, to achieve maximum values of range and endurance, the proper selection and design of the wing airfoil are quite relevant.

The recent forecasts of unmanned aircraft systems (UAS) industry also suggest the future demand for more efficient aircraft capable of flying for longer periods of time and carrying more weight [17]. Therefore, the development of low Re airfoils for such flying machines by using design optimization methodologies can be useful for meeting these future demands. With this motivation, this study focuses on the application of design optimization methods by using an integration of frequently used software XFOIL and lesser-used optimization platform modeFRONTIER. The airfoil design optimization is time-consuming and involves several optimization steps, which must be handled manually. To reduce the number of steps and duration of the optimization process, in this study, the integration of XFOIL with the modeFRONTIER is carried out by developing a code in the modeFRONTIER workflow environment. This software integration methodology for the design optimization of

airfoils significantly improves the efficiency of the process by reducing the steps and time of airfoil optimization.

A step-wise validation of the results was adopted for this study: at first, the XFOIL results were compared with the experimental results which show a good agreement in terms of lift, drag, and moment coefficients with the experimental results. In the second step, the design optimization of the airfoil was performed by using the aforementioned integration approach which manifests an increase of 10% in its optimization parameter. Finally, the characteristics of the optimized airfoil were further compared numerically in ANSYS Fluent; the numerical results re-confirmed the improved aerodynamic characteristics obtained from the design optimization process. The methodology presented in this study can be useful in the future multidisciplinary and efficient designs of the low-speed airfoils.

Most of the design optimization studies focus on transonic optimization due to widespread applications in commercial and military planes. However, low-speed airfoil designs and their optimization has recently become more popular and caught the attention of the researchers mainly due to the UAV applications. In a recent study, Chen [18] essentially utilized the genetic algorithm NSGA-II for the multiple objectives of low-speed optimization. The optimization was mainly performed using CFD for each solution. Only based on the CFD data, the optimal airfoil could be chosen. Though the results were good, however, the evaluation of each airfoil design could be more time consuming primarily because of the CFD based calculations. On the other hand, the optimization methodology proposed in this study is 'quick in use' and efficient. The airfoil is optimized independently using the proposed optimization methodology while only as a secondary measure CFD analysis is used for the further verifications of the characteristics of the (already) optimized airfoil obtained from the proposed optimization method. Liu et al. [19] also utilized the genetic algorithm (NSGA-II) to perform the optimization procedure. For each airfoil of the created population, the analysis was performed on XFOIL. The calculations were performed to obtain the values of the aerodynamic forces for different angles of attack. After the XFOIL analysis, the solution was analyzed using CFD. However, the study itself mentioned that the iteration process during the optimization consumed a high amount of computational resources and time. In a relatively older study conducted in 1987, Maughmer [20], utilized an optimization approach that targeted the same optimization criteria as targeted in this paper. The airfoil was optimized according to its characteristics and operational requirements. The design goals were also set to maximize the lift coefficient while obtaining the minimum drag coefficient. Even though the classical optimization techniques were used, the results of the study were satisfactory, however, they were not verified by any other means which is mainly due to the extremely limited or unavailability of the computational techniques in those days.

Compared to previous studies, the optimization method presented in this paper offers a faster optimization process and utilizes lower computational resources. After validation (with the experimental data), XFOIL was chosen as the aerodynamic solver and was coupled with the software modeFrontier in order to make the optimization procedure automatic and robust. The proposed optimization method also reduces the time for the results validation process as instead of conducting CFD simulations for each geometry (as in the previous studies), only the final and (already) optimized airfoil is recommended to be validated by CFD analysis.

The methodology developed for a 2-dimensional airfoil optimization presented in this study is the first step towards the series of upcoming research work(s). This methodology will be useful for the selection and improvement of the aerodynamic characteristics of the airfoil. The proposed methodology gives the possibility to further optimized the base airfoil, therefore, the proposed airfoil design optimization methodology is the first step in developing the future aircraft/UAV capable of better flight endurance in the years to come. By coupling Xfoil and modeFrontier, the optimization process can be realized in a shorter time with the possibility to adapt or customize the optimization variables. After the process is completed and as per common practice, the final airfoil is validated using CFD. In the future, to analyze the wing performance and aerodynamics, a different method and process can be attempted. Since the proposed methodology presented in this work is valid for a 2-dimensional optimization, which in this case is exclusive for the airfoils only.

This study was carried out under the European Commission ERDF (European Regional Development Fund) project for developing the experimental fluid dynamics facilities including the high-speed wind tunnel at Riga Technical University, Riga, Latvia. This study is also part of the series of studies [21–23] under the mentioned project and will contribute to developing the wind tunnel testing methodologies for small-scale low/high-speed aircraft.

2 Methodology

The development of new airfoils in this work is composed of four steps:

(i) The first step is the selection of typical low Re airfoil for a specific application such as long endurance. The airfoil SG6043 is chosen as the reference airfoil based on its common application in wings when a long-endurance flight is desired
(ii) The second step is the validation of the use of XFOIL as a reliable software for aerodynamics characteris-

tics prediction. This is achieved by comparing the results of the data generated by XFOIL for two airfoils. Airfoils SG6043 and E387 are considered for the investigation because of their widely available wind tunnel results data. The results from the XFOIL are compared with the wind tunnel results presented in [24–27].

(iii) In the third step, the optimization of the airfoil geometry will be performed. Since optimization is done on the basis of C_l, C_d and C_m, XFOIL is used as the aerodynamic solver. The airfoil geometry modification is done by using the Geometry design routine implemented in XFOIL, changing the airfoil's maximum thickness, the position of maximum thickness, maximum camber, the position of maximum camber, and leading-edge radius. modeFRONTIER is used as the optimization software which is coupled with XFOIL, thus automating the iterative process of analyzing different airfoil geometries without the intervention of the user. In addition, the use of a genetic algorithm allows the optimization to follow a path towards the objective and at the same time meeting the constraints. Karman-Tsien compressibility correction is incorporated in XFOIL, which is valid up to the critical Mach number of the airfoil. Beyond that, the accuracy of the results reduces drastically, since it is limited in predicting shock waves and shocked flows. Thus, the maximum Mach number used in this work is limited to 0.5.

(iv) The fourth and final step is the validation of the newly generated airfoil using RANS based simulations in ANSYS Fluent with the transition-sensitive turbulence model γ-Reθ, which allows the assessment of the aerodynamic performance of the airfoil and evaluation of laminar separation bubbles with higher accuracy. The transition SST model utilizes the SST κ–ω transport equations; one equation for intermittency, and one equation for the transition onset. This model is suitable for the flows that develop a boundary layer, which contains a freestream velocity. ANSYS Fluent utilizes an empirical correlation developed by Langtry and Menter, which covers flows in a low freestream turbulence environment [28]. The values of the aerodynamic coefficients obtained in the computational analysis are compared with the results obtained from XFOIL for the optimized airfoil.

This methodology offers a fast and reliable optimization analysis. A significant time reduction is achieved for airfoil optimization. By using modeFRONTIER, a higher number of iterations can be performed in a shorter time. This represents an efficient method that allows the user to have fast and reliable optimization data. Also, by making the process fully automated, a prominent amount of computational resources could be saved, which could also increase the number of analyses performed during a specific amount of time. As previously mentioned, this is possible by establishing the optimization objectives and constraints. The objectives are based on the aerodynamic coefficients of lift, drag, and moment. CFD simulations are only performed for the newly generated optimized airfoil. This offers a significant advantage in terms of computational time by eliminating multiple geometries to be tested in CFD. The main constraint of the proposed method is the limitation of the Mach number. XFOIL contains the Karman–Tsien correction, which has a limit up to the critical Mach number of the airfoil. This study as previously mentioned is limited to (low-speed) subsonic or very early transonic regimes. If a supersonic regime will be used on this methodology, the results will have a lack of accuracy. The methodology is only restricted to low-speed airfoils and focuses on future UAV applications; hence, the methodology fulfills the aim of the investigations i.e. low-speed airfoil optimization.

2.1 Optimization Workflow

Figure 1 demonstrates the workflow environment of the optimization process. In the DOE (design of experiment) module, the initial population is generated. A random sample is created and for each variable, the points are randomly and uniformly distributed. The genetic algorithm used is the NSGA-II (non-dominated sorting genetic algorithm). This algorithm is a fast and superior multi-objective optimization algorithm. It implements a fast non-dominated sorting procedure. The algorithm performs a clever sorting strategy by

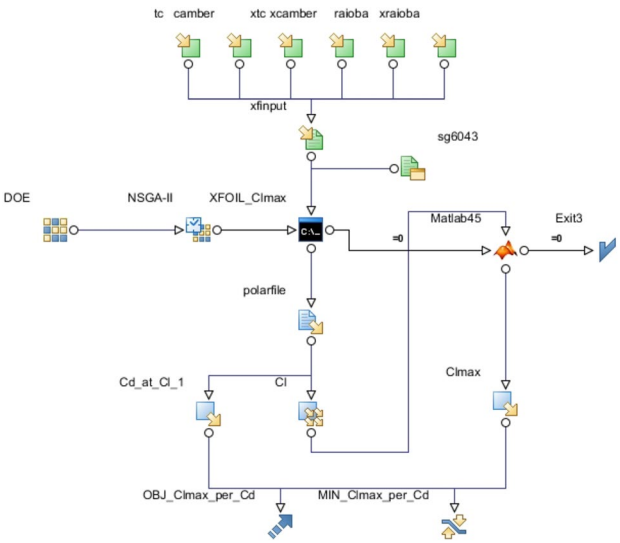

Fig. 1 Optimization workflow

being selective for multi-objective search. The selectiveness that NSGA-II uses, is introduced by storing all non-dominated solutions which so far have been founded from the initial population. For the process, parameter-less diversity preservation is used. The solutions are spread and diverse, without sharing parameters. This is caused by the adoption of a suitable parameter-less approach. It uses the crowding distance, which estimates the density of the solutions in the objective space. Also, the crowded comparison operator is utilized which guides the selection process to a uniformly spread Pareto Frontier. These will be the solutions chosen as optimal, only if an objective could not be improved without sacrificing another one. The NSGA-II algorithm allows continuous (real-coded) and discrete (binary-coded) variables. Continuous variables have a base equal to 0, while discrete variables have a base equal to a positive integer. The original aspect is the application of a genetic algorithm in a field of continuous variables. The version of NSGA-II which is implemented in modeFRONTIER automatically recognizes real-coded and binary-coded variables.

In Fig. 1, green boxes at the top are the input variables, from left to right: maximum thickness (tc), maximum camber (camber), position of the maximum thickness (xtc), position of maximum camber (xcamber), leading-edge radius (raioba) and blending distance from the leading edge (xraioba), respectively. The input variables are linked to the input file "xfinput", which is a text file containing a code which authors specifically developed for the optimization purpose to execute the XFOIL analysis. The output vector "Cl" and the output variable "Cd_at_Cl_1" are connected to the "polarfile", which is a text file that contains the results from XFOIL. The output vector is sent to a MATLAB script that finds the maximum value of C_l and returns it as the output variable "Clmax". The workflow ends with the calculation of the parameter to be maximized.

Aircraft endurance is directly related to the so-called endurance parameter $\left(\frac{C_L^{3/2}}{C_D}\right)$. At first sight, it might be thought that the airfoil having the highest endurance parameter $\left(\frac{C_l^{3/2}}{C_d}\right)$ would offer the best aircraft endurance performance. However, since the airfoil has an impact on the wing area, tail size, and so forth, the airfoil with the highest endurance parameter does not ensure the highest three-dimensional endurance parameter. Because of that, to maximize the aircraft endurance, the airfoil should be designed so that the wing area is decreased by increasing C_{lmax} and reduce section profile drag at the operational lift coefficient. For this work, the operational lift coefficient will be considered equal to 1 for being a common value for aircraft that adopt this type of airfoils. Thus, the parameter to be optimized is:

$$\frac{C_{lmax}}{C_d@C_l=1}.$$

The minimum value of $\frac{C_{lmax}}{C_d@C_l=1}$ is defined as 175.0615, value obtained for the reference airfoil SG6043.

2.2 Computational Methodology

ANSYS 15 CFD modules were used for the comparison of the aerodynamic characteristics of the newly designed and optimized airfoil. The modules used were:

- ICEM CFD—grid generation.
- ANSYS Fluent—case setup and solver.

Several structured grids schemes were generated in a 2D rectangular domain with quadrilateral elements, as shown in Fig. 2a. The domain height was set to 20 chord lengths while the length was set to 30c, the airfoil was positioned in the domain 10c after the inlet, as indicated in Fig. 2b.

In Fig. 2b, the velocity inlets can be identified. At these boundaries, the components of velocity are specified. The magnitude of the velocity was defined to match the Reynolds number of 300,000, considering air

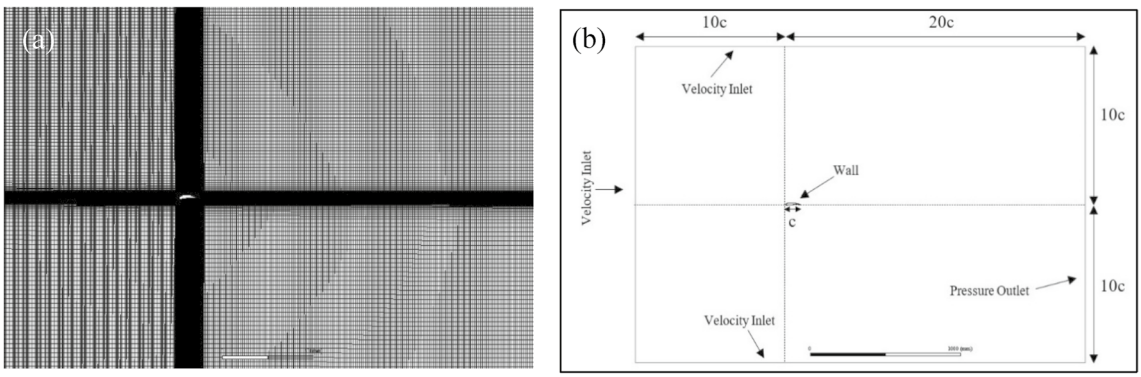

Fig. 2 Domain. **a** Structured mesh; **b** dimensions and boundary conditions

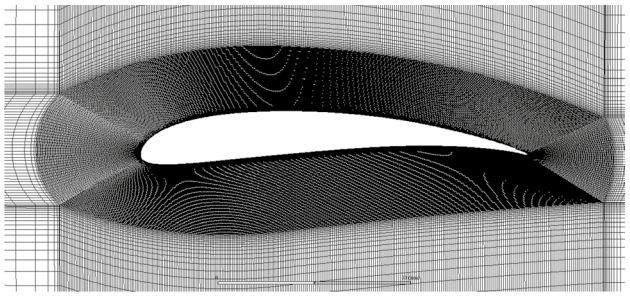

Fig. 3 Structured mesh around the airfoil

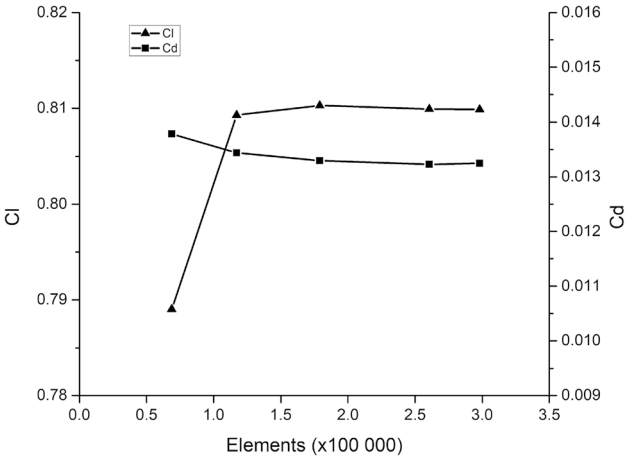

Fig. 4 Grid independence

density at sea level ($\rho = 1.225$ kg/m^3), dynamic viscosity $\mu = 1.7894 \times 10^{-5}$ kg/m s and chord length $c = 0.1$ m. The turbulence conditions are also set at the velocity inlet. As described in [24], the measured turbulence intensity of the wind tunnel where the tests were conducted was 0.1%, thus, the same value was defined for the simulations. At the outlet, the gauge pressure is equal to zero and the airfoil was defined as a wall with the no-slip condition.

A grid independence study was carried out using the optimized airfoil at an angle of attack of 0°, varying the number of nodes in the dense region around the airfoil. The mesh size was increased up to the condition where the values of lift and drag coefficients were nearly constant. This process yielded five different grids schemes; Fig. 3 shows the overall mesh around the airfoil. The height of the first cell adjacent to the airfoil was set to 3.10^{-5} chord length to achieve a $y+$ less than 1, a requirement for the turbulence model chosen for this study i.e. Transition SST (also known as γ-Reθ SST). Figure 4 shows the results of the mesh independence study. In this case, the values for C_l, $C_{d,}$ and C_m were constant after 1700 iterations on the second-order discretization. From this point, the analysis can be considered as "converged", since those values will not change as more iterations are performed. The residuals were set to 1e−06, while the coefficients were considered up to 6 decimals.

It can be seen that the values of lift and drag coefficient are practically constant for a number of elements above approximately 200,000. With that said, all further simulations in this work were carried out with the number of elements above 200,000. In addition, the sweep in angle of attack was done by keeping the airfoil at 0° and inserting the velocity components at the inlet based on the desired angle of attack.

Each simulation starts the calculations using first-order upwind discretization. After 1000 iterations, the discretization is then switched to second-order upwind. Then the simulation runs for up to 2000 iterations or until the values of lift and drag coefficients reach convergence. The pressure–velocity coupling uses a Coupled Scheme for both discretization cases. The Transition SST model utilizes two parameters that are useful in this type of analysis. The first parameter that identifies the state of the flow locally is "gamma". It can have a value between zero and one. When gamma has a value of zero, the flow is locally laminar; while in the case when gamma has a value of one, the flow is fully turbulent. In a case when gamma possesses a value between zero and one, it means that a transitional boundary layer is present. Another way to understand this parameter would be that gamma is the percentage of time when turbulent fluctuations are on the boundary layer. Another applied parameter is Re_θ which is the momentum thickness Reynolds number. The value of Re_θ is calculated in each cell from the transport equation solution. The parameter Re_θ defines the distance from the leading edge where the transition occurs.

3 Results

This section presents the results of the steps mentioned in Sect. 2.

3.1 XFOIL Validation

Since XFOIL is utilized for design optimization purposes, as a first step, the authors conducted a short study to validate the effectiveness of this software. For this, the airfoils SG6043 and E387 were selected because of their widely available wind tunnel results data.

Figure 5 presents a comparison of the experimental and XFOIL results. The results suggest that the aerodynamics coefficients predicted by XFOIL are quite consistent with that obtained from the wind tunnel. Thus, XFOIL is a suitable choice for the evaluation of the performance of an airfoil and a first-hand tool for the design optimization process of this study. In order to calculate Cm, ¼ of the chord was used as the reference point in XFOIL.

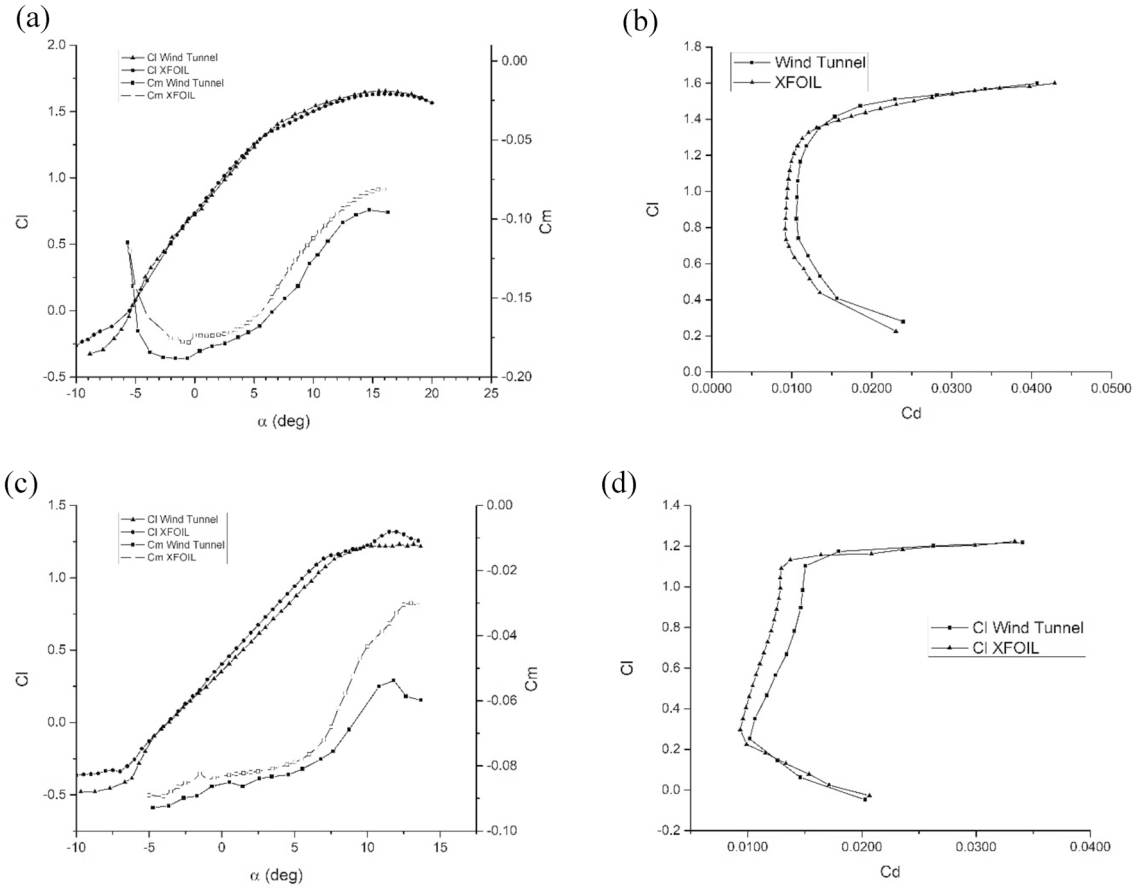

Fig. 5 Comparison of the results of XFOIL predictions with the experimental wind tunnel results. **a** Lift and moment coefficients versus angle of attack for SG6043 at Re = 300,000; **b** drag polar for SG6043 at Re = 300,000; **c** lift and moment coefficients versus angle of attack for E387 at Re = 200,000; **d** drag polar for E387 at Re = 200,000

3.2 Design Optimization

For the optimization of the airfoil geometry, XFOIL was integrated into the modeFRONTIER work environment as the aerodynamic solver. This integration methodology of two software automated the iterations for several geometries of the base airfoil i.e. SG6043 without user intervention. Using this integrated environment, approximately 2600 iterations were needed to reach convergence. Figure 6 shows the design history of the objective of the optimization, i.e. $\frac{C_{\text{lmax}}}{C_{\text{d}}@C_{\text{l}}=1}$. The graph only shows the feasible designs, meaning that only the airfoils that have a ratio $\frac{C_{\text{lmax}}}{C_{\text{d}}@C_{\text{l}}=1}$ greater than 175.0615 (optimization constraint) are shown. A maximum value of 192.55, which is approximately 10% greater than the value of 175.0616 obtained for the SG6043 airfoil.

Table 1 shows the comparison between geometric parameters of the base SG6043 airfoil and the new optimized airfoil. For convenience, the authors named this modified airfoil SG6043mod and will be used throughout this study.

To better visualize the airfoils, Fig. 7 plots both airfoils with their normalized y and x coordinates.

It is possible to see that the SG6043mod's maximum thickness is greater than the SG6043's. The position of maximum thickness has moved frontwards (closer to the leading edge), while the position of maximum camber has moved rearwards (closer to the trailing edge). The SG6043mod is slightly more cambered than the SG6043. Lastly, the leading edge radius of the SG6043mod is greater than the SG6043's radius. The effect of these geometric parameters can be visualized in terms of lift, drag and pressure coefficients and boundary layer behavior. Figure 8 shows the plot of the lift coefficient against the angle of attack.

The most notable differences between the airfoils are the SG6043mod greater values of $C_{l_{\text{max}}}$ and stall angle i.e. 1.7968 at 17.5° against 1.6326 at 16° of the SG6043. This increase can be explained by the increase in thickness, camber, and leading-edge radius. Thicker airfoils also have thicker boundary layers (i.e. more turbulent), which makes it more resistant to the adverse pressure gradient, allowing the airfoil to reach higher angles of attack. Besides that, with

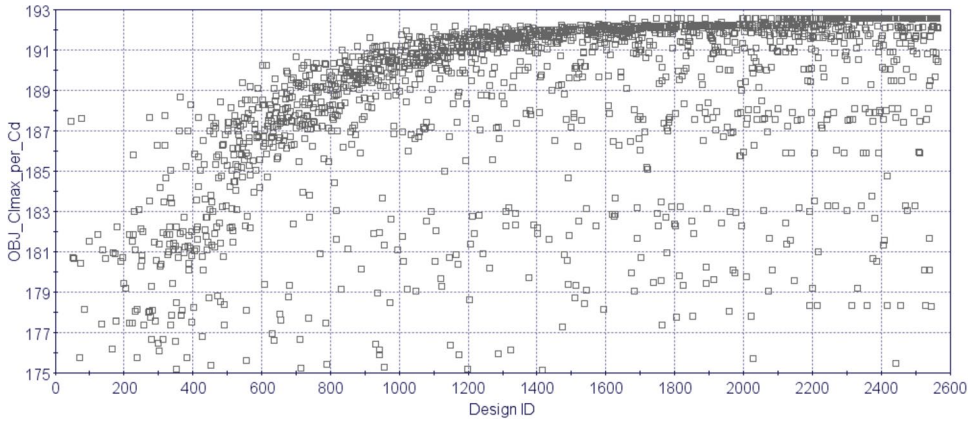

Fig. 6 Optimization objective versus iterations

Table 1 Geometric parameters comparison

Airfoil	Max t/c	Position of max t/c	Camber	Position of max camber	LE radius
SG6043	10.00%	32.32%	5.50%	50.50%	1.69%
SG6043 mod	11.90%	23.23%	6.00%	52.52%	2.17%

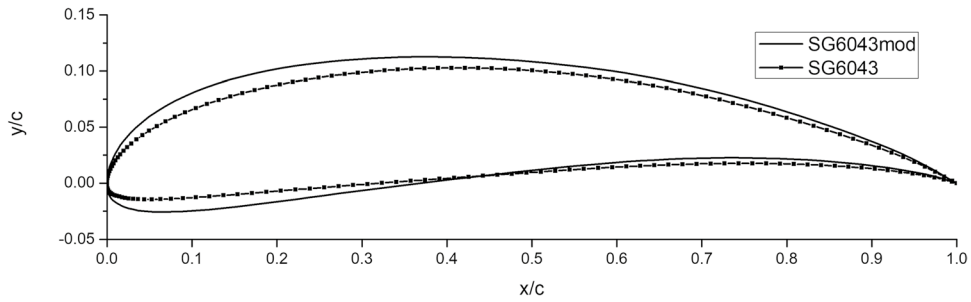

Fig. 7 SG6043 and SG6043mod

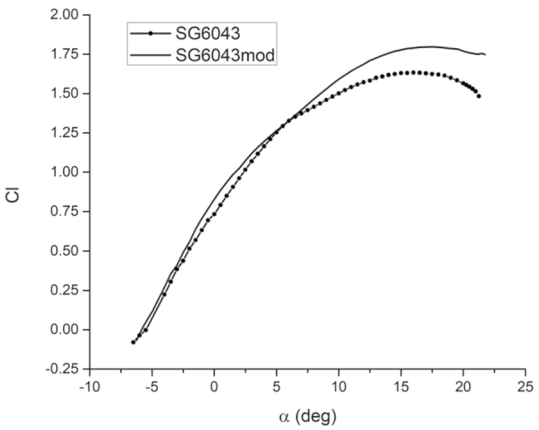

Fig. 8 C_l versus angle of attack for SG6043 and SG6043mod airfoils

more camber, there is a better "alignment" of the leading edge with the flow at higher angles of attack, thus lowering the suction peak on the upper surface and reducing the adverse pressure gradient. The increased leading edge radius also lowers the suction peak. The lower suction peak of the SG6043mod airfoil can be seen on the pressure coefficient graph at 16 degrees shown in Fig. 9. The value of zero lift angle (α_0) of SG6043mod is slightly more negative than the SG6043's, which is an effect mainly caused by the increased camber. The same goes for the increased value of C_{l_0}, which is greater for the SG6043mod. In terms of stall behavior, both airfoils presented gentle stalling characteristics, without subtle changes in lift coefficient after the stall angle.

In Fig. 9a, it is possible to see that for an angle of attack of 16°, the transition from laminar to turbulent for the SG6043 occurs at 0.038c, while for the SG6043mod it occurs at 0.092c. Besides that, when the C_p distribution is almost horizontal on the upper surface, it shows the occurrence of flow separation. One can identify the separation by examining a magnified C_p graph in Fig. 9b. For the SG6043, separation occurs at around 0.6*c*, while for the SG6043mod it occurs further away at around 0.66*c*. With less turbulent and separated flow, the SG6043mod at 16° should have less

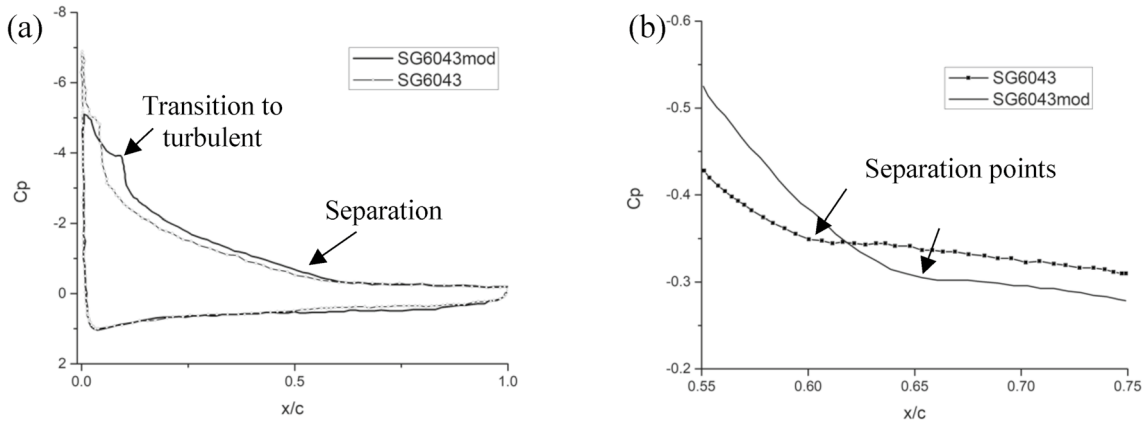

Fig. 9 **a** C_p distribution at $\alpha = 16°$; **b** Magnified C_p distribution

drag, which is consistent with the results. At 16 degrees, SG6043 has $C_d = 0.074$ and SG6043mod has $C_d = 0.065$. Nevertheless, it is not sufficient to analyze the drag coefficient for only one point. Thus, the drag polar for the airfoil is plotted in Fig. 10.

It is possible to note two regions where SG6043 drag coefficient is smaller than SG6043mod; $0.35 < C_l < 0.995$ and $1.053 < C_l < 1.43$. However, the differences are in the order of 0.002–0.003 in these regions. For values of C_l above 1.43 up to SG6043 $C_{l_{max}}$, it has higher values of drag coefficient, due to separation that likely has already started at this point. In addition to that, SG6043mod reaches higher values of C_l, which has already been observed in Fig. 8. The purpose of Fig. 10b is to illustrate the drag coefficient values when the lift coefficient has a value of 1. In this case, SG6043mod has a slightly lower C_d when $C_l = 1$. Figure 10b is a 'zoomed-in' version of Fig. 10a. Figure 10b is taken from the region inside the red box in Fig. 10a. The 'red box' region in Fig. 10a is demonstrated in Fig. 10b and shows the insight of the two curves. As it can be observed in Fig. 10a, the curves cross each other at several points. This means that each airfoil has a better C_l to C_d ratio, depending on the value of lift or drag on which we are looking. So, Fig. 10b focuses on the value of $C_l = 1$. At this point, SG6043mod has a lower value of drag compared to SG6043. Now examining the value of the drag coefficient for $C_l = 1$, the design point, SG6043mod demonstrates slightly lower values, which can be seen in Fig. 10b. For $0.995 < C_l < 1.053$, SG6043mod drag coefficient is slightly smaller than SG6043. From the lift coefficient and drag polar graphs, one can observe the strategy adopted by the optimization algorithm, minimize the drag coefficient at $C_l = 1$ while increasing the value of $C_{l_{max}}$. This is consistent with the parameter that had to be maximized: $\frac{C_{lmax}}{C_d @ C_l = 1}$.

In terms of the moment coefficient, SG6043mod presented higher values, as shown in Fig. 11.

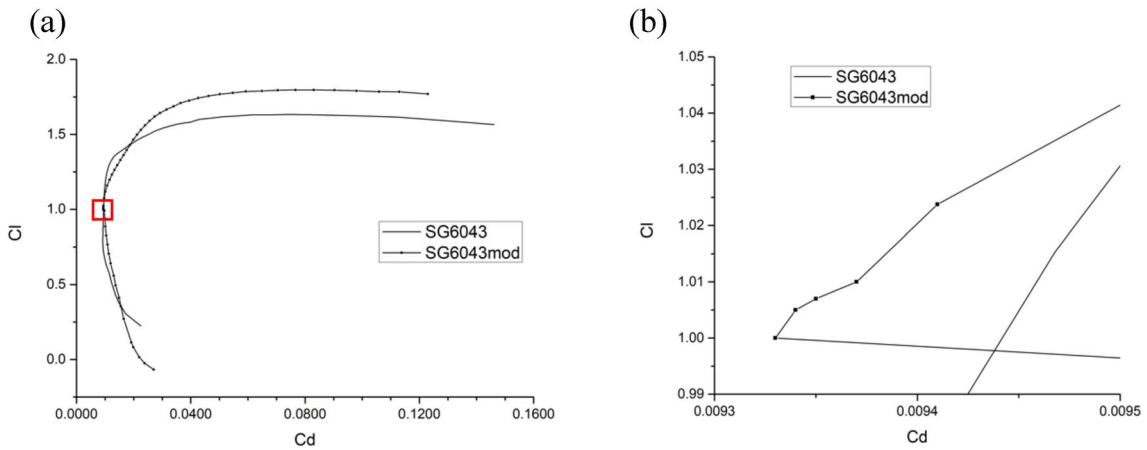

Fig. 10 **a** Drag polar of SG6043 and SG6043mod airfoils; **b** drag polar around the design point; **c** drag polar around the design point with different axis values

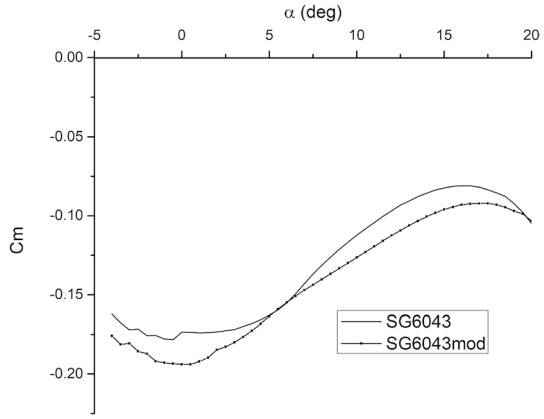

Fig. 11 C_m versus angle of attack for SG6043 and SG6043mod airfoils

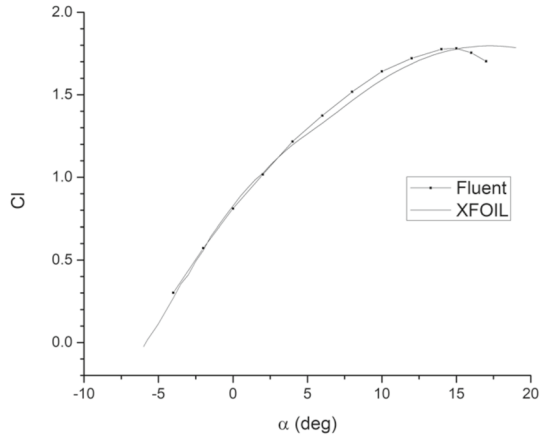

Fig. 12 Lift coefficient of SG6043mod obtained by Fluent and XFOIL

This characteristic is related to the increased camber of the SG6043mod airfoil. Airfoils with higher cambers tend to present higher aerodynamic loads closer to the trailing edge, which increases the nose-down moment.

3.3 Numerical Simulations

Figure 12 shows the plot of lift coefficient versus angle of the attack obtained by the numerical simulations in ANSYS Fluent and compared to the results obtained by XFOIL. Even though Fluent predicted an earlier stall in comparison to XFOIL, the overall comparison is highly accurate.

Table 2 summarizes the comparison between Fluent and XFOIL results.

The drag polar obtained from XFOIL and Fluent simulations is plotted in Fig. 13.

Table 2 Fluent and XFOIL results comparison

Parameter	Fluent	XFOIL
$C_{l_{max}}$	1.7814	1.7968
α stall (degrees)	15	17.5
C_{l_0}	0.8099	0.8271

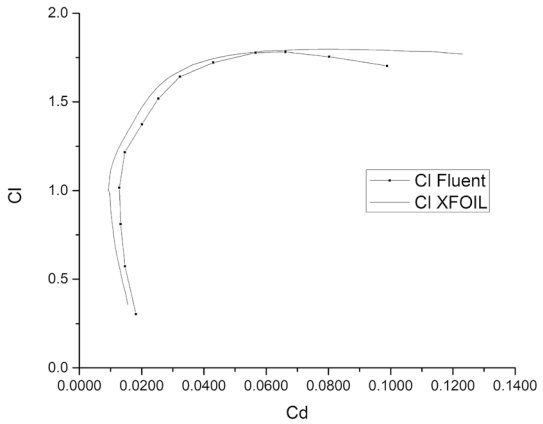

Fig. 13 Drag polar for SG6043mod, obtained by XFOIL and Fluent

The drag coefficient of numerical simulations is higher than the one predicted by XFOIL for the entire curve. Nevertheless, the values predicted by XFOIL are very close to the ones obtained by Fluent; differences are only in the order of 30 drag counts (i.e. 0.0030), which are minor and negligible.

The formation of laminar separation bubbles (LSB) is predicted by Fluent and it was observed that, as the angle of attack is increased, the bottom surface bubble disappears, while the top surface bubble moves towards the leading edge, as displayed in Fig. 14 where the LSB can be seen at different angles of attack, with a close-up of each region. Laminar separation bubbles have also been detected for low Reynolds number in the works of Hübbe [11] and Aftab et al. [29].

Inside the separation bubbles, the flow is reversed, which creates a dead zone. In practice, the bubbles increase the local thickness of the airfoil, which usually increases the drag. The reversed flow inside the bottom surface bubble can be seen in Fig. 15.

Figure 16 shows the pressure coefficient distribution for the same angles of attack as in Fig. 14. In every pressure coefficient distribution, a plateau followed by a sudden decrease in the curve can be observed. This is indicative of laminar separation bubbles with a turbulent reattachment. For higher angles of attack, it is notable that there is the same plateau near the trailing edge, which indicates flow separation. It is also possible to note that this plateau moves

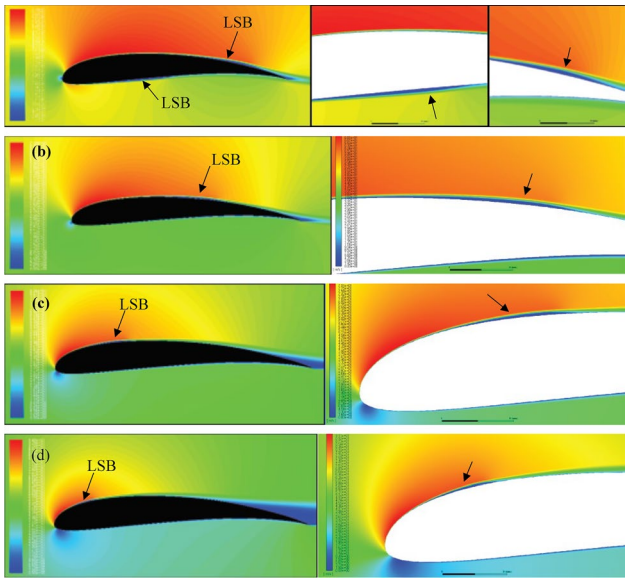

Fig. 14 Velocity contour for SG6043mod. **a** $\alpha = 0°$; **b** $\alpha = 4°$; **c** $\alpha = 8°$; **d** $\alpha = 12°$

towards the leading edge as the angle of attack increases, in agreement with the velocity contours shown in Fig. 14. At an angle of attack equal to zero Fig. 16a, the bottom surface also has a plateau followed by a sudden decrease in pressure coefficient, indicating another laminar separation bubble.

Plots of the skin friction coefficient along the chord can be very helpful to identify the length of the bubbles and transition and reattachment points. Figure 17 displays the skin friction coefficient along the chord for the same angles of attack that have been discussed so far. For the angle of attack zero Fig. 17a), the skin friction coefficient for both surfaces has been plotted due to the presence of two laminar separation bubbles. For the further angles of attack Fig. 17b–d, only the skin friction coefficient of the top surface has been plotted, since the bubble on the bottom surface disappears. The length of the bubble can be estimated by identifying the positions of laminar separation and turbulent reattachment. Table 3 summarizes the laminar separation bubble behavior for different angles of attack.

The moment coefficient versus angle of attack obtained by XFOIL and Fluent is illustrated in Fig. 18. XFOIL and Fluent predictions show good agreement at low angles of attack (from $-4°$ to $2°$). The difference grows, as the angle of attack increases, with XFOIL slightly underestimating the values of the moment coefficient. Nevertheless, the overall differences in C_m for higher angles of attack are negligible and the curves demonstrate a similar trend, with the curve

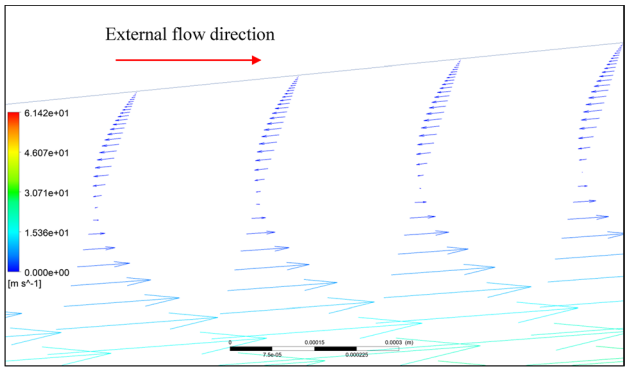

Fig. 15 Vectors of velocity inside the bottom surface bubble for SG6043mod

predicted by XFOIL with a more positive derivative between $0°$ and $15°$.

4 Discussion and Conclusions

In this work, design optimization of a low Reynolds number airfoil was performed by the integration of two software i.e. modeFRONTIER and XFOIL. The newly generated airfoil demonstrated improved aerodynamic characteristics in comparison to the reference airfoil. Numerical simulations in ANSYS reconfirmed the improved results obtained from the proposed optimization methodology.

The airfoil design is often a time-consuming and iterative process. The proposed software integration methodology for the design optimization of airfoils significantly improved the efficiency of the process by reducing the steps and time of airfoil optimization. The optimization method proposed in this study can be useful because its multidisciplinary nature of the optimization allows the user to define different requirements that are not only related to the aerodynamic features but also to geometric constraints. The proposed methodology can be considered as a universal approach for optimizing the airfoils with particular features in terms of geometry; for example, the minimum value of the internal volume of a wing can be a constraint in some applications, in that case, the thickness of the airfoil can be limited to a specific value or becomes a potential design goal. Hence, by using the proposed optimization methodology, the user can easily adapt according to the design goals and constraints without any additional steps.

From the numerical simulations, the newly generated airfoil presents better 2D aerodynamic characteristics than

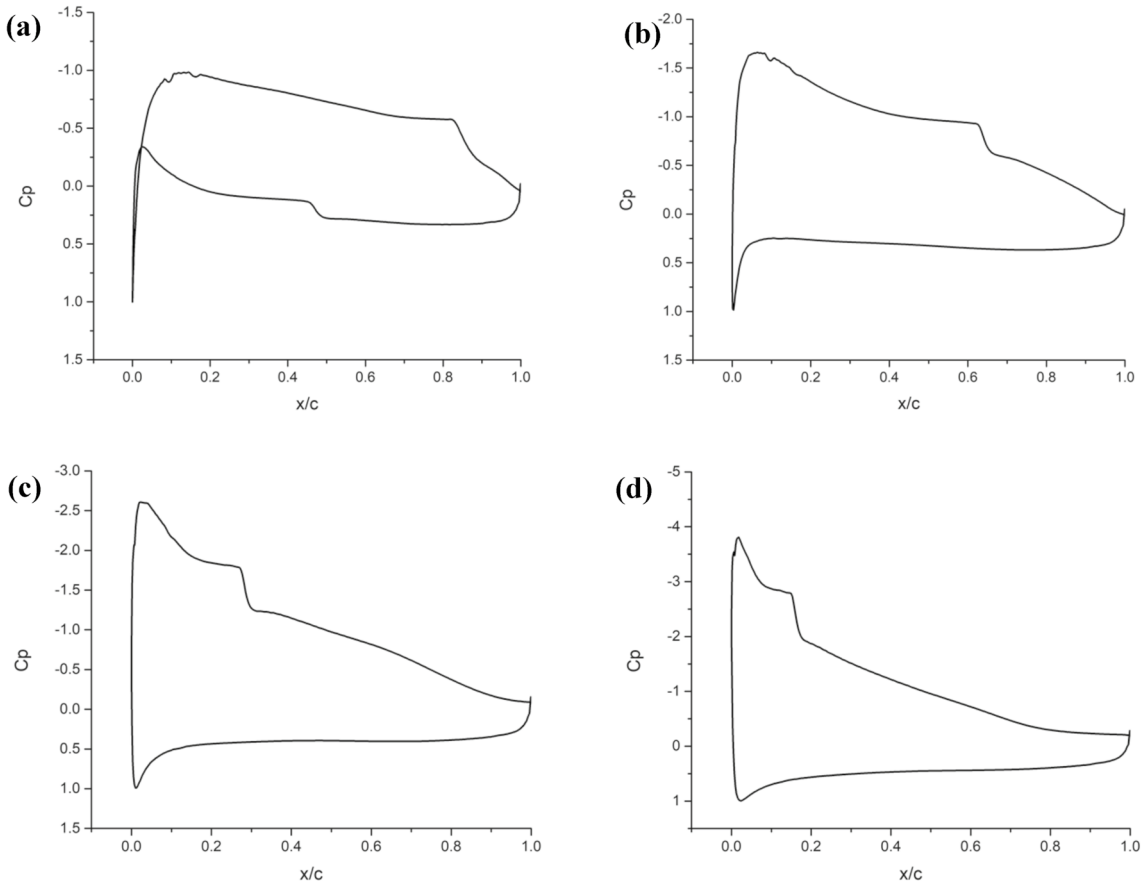

Fig. 16 C_p distribution for SG6043mod. **a** 0°; **b** 4°; **c** 8°; **d** 12°

the reference airfoil. Since SG6043mod has been optimized based on the parameter $\frac{C_{\text{lmax}}}{C_{\text{d}}@C_{\text{l}}=1}$, it can be applied for long-endurance UAVs with a design lift coefficient around 1, due to its improved values of C_{lmax} and $C_{\text{d}}@C_{\text{l}} = 1$. In addition to UAVs, the newly generated airfoil can also be a potential candidate for general aviation purposes operating within the range of low Reynolds numbers.

Since the numerical simulations are also associated with their particular limitations, the authors believe that further/final evaluation of the airfoil should be done with wind tunnel testing. To widen the scope of the present work, in the future, alongside wind tunnel testing, an analysis of the general endurance parameter would also be included in future studies. Since the general endurance parameter is influenced by wing aspect ratio, weight, 3D drag polar, and other parameters. a detailed process would be established to ensure the accuracy of the analysis by designing (two) wings from the airfoil. The analysis of both wings using SG6043 and SG6043mod as a base and optimized airfoils will determine real-life applications, where 3D characteristics are the most relevant when it comes to the performance evaluation of a wing and aircraft. Nevertheless, improved 2D aerodynamic characteristics of the airfoil SG6043mod is a starting point for long endurance flights of aircraft.

Following conclusions can be drawn from the study:

(i) The airfoil design optimization methodology presented in this study by the integration of XFOIL in modeFRONTIER is flexible and efficient with significantly reducing the time associated with the conventional optimization process.
(ii) The optimized airfoil showed significant improvements in the optimization parameters (10% increase in $\frac{C_{\text{lmax}}}{C_{\text{d}}@C_{\text{l}}=1}$); hence, design optimization targets were met which demonstrates the effectiveness of the proposed optimization methodology of this study.
(iii) The proposed design optimization method can be useful for a variety of applications and required aerodynamic characteristics.

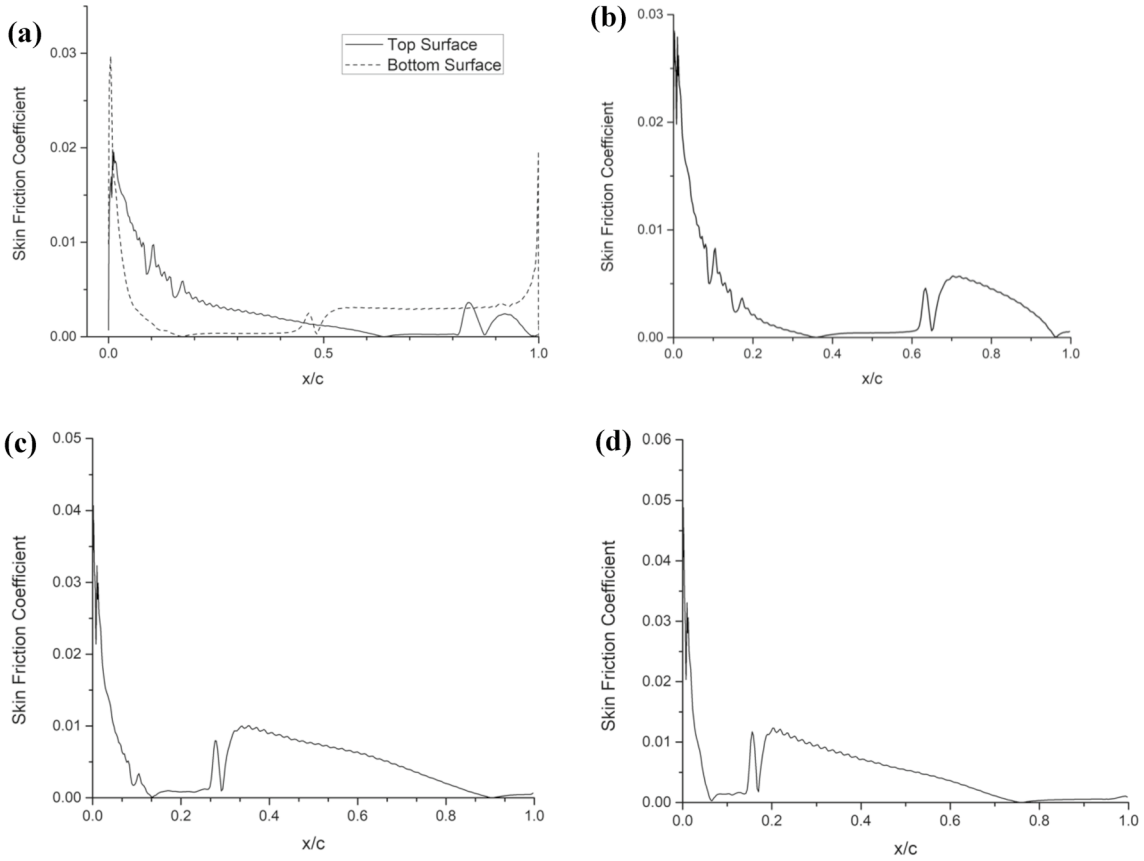

Fig. 17 Skin friction coefficient for SG6043mod. **a** $\alpha = 0^{\circ}$; **b** $\alpha = 4^{\circ}$; **c** $\alpha = 8^{\circ}$; **d** $\alpha = 12^{\circ}$

Table 3 Position of laminar separation and turbulent reattachment and bubble length

α (deg)	Laminar separation (x/c)	Turbulent reattachment (x/c)	Length (x/c)
0	Top = 0.645	Top = 0.87	Top = 0.225
	Bottom = 0.17	Bottom = 0.48	Bottom = 0.31
4	0.36	0.65	0.29
8	0.135	0.29	0.155
12	0.064	0.17	0.106

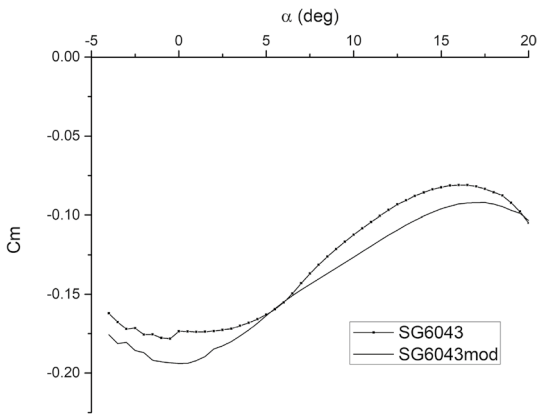

Fig. 18 C_m versus angle of attack obtained by XFOIL and Fluent for SG6043mod

(iv) For the low Reynolds number airfoils, XFOIL provided good agreement with the experimental results and proved to be a reliable tool. However, future investigations on the high lift airfoils using XFOIL are recommended and planned.

(v) Numerical results of the newly generated airfoil confirm the improved aerodynamic characteristics. UAVs are the potential applications of the newly generated airfoil while it can also be considered for general aviation applications.

(vi) Further evaluation of the airfoil using wind tunnel testing is recommended and planned.

Acknowledgements This work has been supported by the European Regional Development Fund within the Activity 1.1.1.2 "Post-doctoral Research Aid" of the Specific Aid Objective 1.1.1 "To increase the research and innovative capacity of scientific institutions of Latvia and the ability to attract external financing, investing in human resources and infrastructure" of the Operational Program "Growth and Employment" (No. 1.1.1.2/VIAA/2/18/321).

References

1. Mueller TJ (1985) Low Reynolds number vehicles, AGARD-AG-288
2. Gross A, Fasel H (2010) Numerical investigation of separation for airfoils at low Reynolds number. In: 40th fluid dynamics conference and exhibit, Chicago
3. Kessler DA, Johnson R, Corrigan AT, Qidwai S, Merril S, Thomas J (2016) Modeling low-Reynolds-number flow over rough airfoils. In: 54th AIAA aerospace sciences meeting, San Diego
4. Drela M (1989) XFOIL: an analysis and design system for low Reynolds number airfoils. Springer, Cambridge
5. Katz J (2019) Classical and potential flow based aerodynamics - do we need them? In: AIAA Scitech 2019 Forum, San Diego
6. Buckley HP, Zhou BY, Zingg DW (2010) Airfoil optimization using practical aerodynamic design requirements. J Aircr 47(5):1707–1719
7. Tirado EM, Quagliarella D, Tognaccini R (2019) Airfoil optimization using far-field analysis of the drag force. In: AIAA Scitech 2019 forum, San Diego
8. Ferreira CS, Barone MF, Zanon A, Kemp R, Giannattasio P (2015) Airfoil optimization for stall regulated vertical axis wind turbines. In: 33rd wind energy symposium, Kissimmee
9. Hájek J (2009) Aerodynamic optimization of airfoils and wings using fast solver. Prague: Ph.D. Dissertation
10. Menter FR, Langtry R, Völker S (2006) Transition modelling for general purpose CFD codes. Flow Turbul Combust 77(1–4):277–303
11. Hübbe GBB (2017) Numerical and experimental analysis of a high lifting airfoil at low Reynolds number flows, Florianópolis. Master Thesis
12. Mushynski AT, Johnson T (2017) Analysis and design of a low reynolds propeller for optimal unmanned aerial vehicle (UAV) flight. In: ASME 2017 international mechanical engineering congress and exposition, Tampa
13. Holst D, Church B, Pechlivanoglou G, Tüzüner E, Saverin J, Nayeri CN, Paschereit CO (2018) Experimental analysis of a NACA 0021 airfoil section through 180-degree angle of attack at low Reynolds numbers for use in wind turbine analysis. J Eng Gas Turbines Power 9
14. Brandt JB, Selig MS (2011) Propeller performance data at low Reynolds numbers. In: 49th AIAA aerospace sciences meeting, Orlando
15. Dähnert J, Lyko C, Peitsch D (2013) Transition mechanisms in laminar separated flow under simulated low pressure turbine aerofoil conditions. J Turbomach 135(1)
16. Désert T, Moschetta J, Bézard H (2018) Numerical and experimental investigation of an airfoil design for a Martian micro rotorcraft. Int J Micro Air Veh 10(3):262–272
17. Federal Aviation Administration (2019) Aerospace forecast 2019–2039
18. Chen X, Agarwal RK (2014) Shape optimization of airfoils in transonic flow using a multi-objective genetic algorithm. J Aerosp Eng
19. Liu Z, Dong L, Moschetta J-M, Zhao J, Yan G (2014) Optimization of nano-rotor blade airfoil using controlled elitist NSGA-II. Int J Micro Air Veh 6
20. Maughmer MD, Somers DM (1987) The design of an airfoil for a high-altitude, long-endurance remotely piloted vehicle. In: 5th applied aerodynamics conference, Monterey
21. Arshad A, Samarasinghe S, Ameer MAF, Urbahs A (2020) A simplified design approach for high-speed wind tunnels. Part I: table of inclination. J Mech Sci Technol 34(6):2455–2468
22. Arshad A, Samarasinghe S, Kovalcuks V (2020) A simplified design approach 28 for high-speed wind tunnels. Part-I.I: optimized design of settling chamber and inlet nozzle. In: IEEE 11th international conference on mechanical and aerospace engineering (ICMAE), pp 150–154
23. Arshad A, Andrew N, Blumbergs I (2020) Computational study of noise reduction in CFM56–5B using core nozzle chevrons. In: IEEE 11th international conference on mechanical and aerospace engineering (ICMAE), pp 162–167
24. Selig MS, Guglielmo JJ, Broeren AP, Giguère P (1995) Summary of low-speed airfoil data, vol 1. Soartech Publications, Virginia Beach
25. Selig MS, Guglielmo JJ, Giguère P, Lyon CA, Ninham CP (1996) Summary of low-speed airfoil data, vol 2. Soartech Publications, Virginia Beach
26. Selig MS, Lyon CA, Broeren AP, Giguère P, Gopalarathnam A (1997) Summary of low-speed airfoil data, vol 3. Soartech Publications, Virginia Beach
27. Selig MS, Williamson GA, McGranahan BD, Broughton BA, Deters RW, Brandt JB (2012) Summary of low-speed airfoil data, vol 5
28. ANSYS, Inc. Fluent Theory Guide, Release 19.2
29. Aftab SMA, Rafie ASM, Razak NA, Ahmad KA (2016) Turbulence model selection for low Reynolds number flows. PLoS ONE 11(4):e0153755